Astronomy & Astrophysics manuscript no. output
September 20, 2025

Euclid Quick Data Release (Q1)

An investigation of optically faint, red objects in the Euclid Deep Fields

Euclid Collaboration: G. Girardi[⋆1,2], G. Rodighiero[1,2], L. Bisigello[2], A. Enia[3,4], A. Grazian[2], E. Dalla Bontà[1,2,5], E. Daddi[6], S. Serjeant[7], G. Gandolfi[8,2], C. C. Lovell[9], K. I. Caputi[10,11], A. Bianchetti[1,2], A. Vietri[1], N. Aghanim[12], B. Altieri[13], A. Amara[14], S. Andreon[15], N. Auricchio[4], H. Aussel[6], C. Baccigalupi[16,17,18,19], M. Baldi[3,4,20], A. Balestra[2], S. Bardelli[4], P. Battaglia[4], R. Bender[21,22], A. Biviano[17,16], A. Bonchi[23], E. Branchini[24,25,15], M. Brescia[26,27], J. Brinchmann[28,29], S. Camera[30,31,32], G. Cañas-Herrera[33,34,35], V. Capobianco[32], C. Carbone[36], J. Carretero[37,38], S. Casas[39], M. Castellano[40], G. Castignani[4], S. Cavuoti[27,41], K. C. Chambers[42], A. Cimatti[43], C. Colodro-Conde[44], G. Congedo[45], C. J. Conselice[46], L. Conversi[47,13], Y. Copin[48], F. Courbin[49,50], H. M. Courtois[51], M. Cropper[52], A. Da Silva[53,54], H. Degaudenzi[55], G. De Lucia[17], A. M. Di Giorgio[56], C. Dolding[52], H. Dole[12], F. Dubath[55], C. A. J. Duncan[46], X. Dupac[13], S. Dusini[57], A. Ealet[48], S. Escoffier[58], M. Farina[56], R. Farinelli[4], F. Faustini[23,40], S. Ferriol[48], F. Finelli[4,59], S. Fotopoulou[60], M. Frailis[17], E. Franceschi[4], S. Galeotta[17], K. George[22], B. Gillis[45], C. Giocoli[4,20], P. Gómez-Alvarez[61,13], J. Gracia-Carpio[21], B. R. Granett[15], F. Grupp[21,22], S. Gwyn[62], S. V. H. Haugan[63], W. Holmes[64], I. M. Hook[65], F. Hormuth[66], A. Hornstrup[67,68], P. Hudelot[69], K. Jahnke[70], M. Jhabvala[71], E. Keihänen[72], S. Kermiche[58], A. Kiessling[64], B. Kubik[48], K. Kuijken[35], M. Kümmel[22], M. Kunz[73], H. Kurki-Suonio[74,75], Q. Le Boulc'h[76], A. M. C. Le Brun[77], D. Le Mignant[78], S. Ligori[32], P. B. Lilje[63], V. Lindholm[74,75], I. Lloro[79], G. Mainetti[76], D. Maino[80,36,81], E. Maiorano[4], O. Mansutti[17], S. Marcin[82], O. Marggraf[83], M. Martinelli[40,84], N. Martinet[78], F. Marulli[85,4,20], R. Massey[86], S. Maurogordato[87], E. Medinaceli[4], S. Mei[88,89], M. Melchior[90], Y. Mellier[91,69], M. Meneghetti[4,20], E. Merlin[40], G. Meylan[92], A. Mora[93], M. Moresco[85,4], L. Moscardini[85,4,20], R. Nakajima[83], C. Neissner[94,38], S.-M. Niemi[33], J. W. Nightingale[95], C. Padilla[94], S. Paltani[55], F. Pasian[17], K. Pedersen[96], W. J. Percival[97,98,99], V. Pettorino[33], S. Pires[6], G. Polenta[23], M. Poncet[100], L. A. Popa[101], L. Pozzetti[4], F. Raison[21], R. Rebolo[44,102,103], A. Renzi[1,57], J. Rhodes[64], G. Riccio[27], E. Romelli[17], M. Roncarelli[4], E. Rossetti[3], B. Rusholme[104], R. Saglia[22,21], Z. Sakr[105,106,107], D. Sapone[108], B. Sartoris[22,17], J. A. Schewtschenko[45], M. Schirmer[70], P. Schneider[83], M. Scodeggio[36], A. Secroun[58], G. Seidel[70], S. Serrano[109,110,111], P. Simon[83], C. Sirignano[1,57], G. Sirri[20], L. Stanco[57], J. Steinwagner[21], P. Tallada-Crespí[37,38], D. Tavagnacco[17], A. N. Taylor[45], H. I. Teplitz[112], I. Tereno[53,113], S. Toft[11,114], R. Toledo-Moreo[115], F. Torradeflot[38,37], I. Tutusaus[106], L. Valenziano[4,59], J. Valiviita[74,75], T. Vassallo[22,17], G. Verdoes Kleijn[10], A. Veropalumbo[15,25,24], Y. Wang[112], J. Weller[22,21], A. Zacchei[17,16], G. Zamorani[4], F. M. Zerbi[15], I. A. Zinchenko[22], E. Zucca[4], V. Allevato[27], M. Ballardini[116,117,4], M. Bolzonella[4], E. Bozzo[55], C. Burigana[118,59], R. Cabanac[106], A. Cappi[4,87], D. Di Ferdinando[20], J. A. Escartin Vigo[21], L. Gabarra[119], M. Huertas-Company[44,120,121,122], J. Martín-Fleitas[93], S. Matthew[45], N. Mauri[43,20], R. B. Metcalf[85,4], A. Pezzotta[21], M. Pöntinen[74], C. Porciani[83], I. Risso[123], V. Scottez[91,124], M. Sereno[4,20], M. Tenti[20], M. Viel[16,17,19,18,125], M. Wiesmann[63], Y. Akrami[126,127], I. T. Andika[128,129], S. Anselmi[57,1,130], M. Archidiacono[80,81], F. Atrio-Barandela[131], C. Benoist[87], K. Benson[52], D. Bertacca[1,2,57], M. Bethermin[132], A. Blanchard[106], L. Blot[133,130], M. L. Brown[46], S. Bruton[134], A. Calabro[40], B. Camacho Quevedo[109,111], F. Caro[40], C. S. Carvalho[113], T. Castro[17,18,16,125], F. Cogato[85,4], A. R. Cooray[135], O. Cucciati[4], S. Davini[25], F. De Paolis[136,137,138], G. Desprez[10], A. Díaz-Sánchez[139], J. J. Diaz[44], S. Di Domizio[24,25], J. M. Diego[140], P.-A. Duc[132], Y. Fang[22], A. G. Ferrari[20], P. G. Ferreira[119], A. Finoguenov[74], A. Fontana[40], F. Fontanot[17,16], A. Franco[137,136,138], K. Ganga[88], J. García-Bellido[126], T. Gasparetto[17], V. Gautard[141], E. Gaztanaga[111,109,9], F. Giacomini[20], F. Gianotti[4], G. Gozaliasl[142,74], A. Gregorio[143,17,18], M. Guidi[3,4], C. M. Gutierrez[144], A. Hall[45], W. G. Hartley[55], S. Hemmati[104], C. Hernández-Monteagudo[103,44], H. Hildebrandt[145], J. Hjorth[96], J. J. E. Kajava[146,147], Y. Kang[55], V. Kansal[148,149], D. Karagiannis[116,150], K. Kiiveri[72], C. C. Kirkpatrick[72], S. Kruk[13], J. Le Graet[58], L. Legrand[151,152], M. Lembo[116,117], F. Lepori[153], G. Leroy[154,86], G. F. Lesci[85,4], J. Lesgourgues[39], L. Leuzzi[85,4], T. I. Liaudat[155], A. Loureiro[156,157], J. Macias-Perez[158], G. Maggio[17], M. Magliocchetti[56], E. A. Magnier[42], F. Mannucci[159], R. Maoli[160,40], C. J. A. P. Martins[161,28], L. Maurin[12], M. Miluzio[13,162], P. Monaco[143,17,18,16], C. Moretti[19,125,17,16,18], G. Morgante[4], S. Nadathur[9], K. Naidoo[9], A. Navarro-Alsina[83], S. Nesseris[126], F. Passalacqua[1,57], K. Paterson[70], L. Patrizii[20], A. Pisani[58,163], D. Potter[153], S. Quai[85,4], M. Radovich[2], P.-F. Rocci[12], S. Sacquegna[136,137,138], M. Sahlén[164], D. B. Sanders[42], E. Sarpa[19,125,18], C. Scarlata[165], J. Schaye[35], A. Schneider[153], M. Schultheis[87], D. Sciotti[40,84], E. Sellentin[166,35], F. Shankar[167], L. C. Smith[168], J. Stadel[153], K. Tanidis[119], C. Tao[58], G. Testera[25], R. Teyssier[163],

S. Tosi[24,123], A. Troja[1,57], M. Tucci[55], C. Valieri[20], A. Venhola[169], D. Vergani[4], G. Verza[170], P. Vielzeuf[58], N. A. Walton[168], and D. Scott[171]

(Affiliations can be found after the references)

September 20, 2025

ABSTRACT

Our understanding of cosmic star formation at $z > 3$ used to largely rely on rest-frame UV observations. However, these observations overlook dusty and massive sources, resulting in an incomplete census of early star-forming galaxies. Recent infrared data from *Spitzer* and the *James Webb* Space Telescope (JWST) have revealed a hidden population at $z \sim 3$–6 with extreme red colours.

Taking advantage of the overlap between imaging of the Euclid Deep Fields (EDFs), covering about 60 deg^2, and ancillary *Spitzer* observations, we identified 27 000 extremely red objects with $H_E - \mathrm{IRAC2} > 2.25$ (dubbed HIEROs) down to a $10\,\sigma$ completeness magnitude limit of IRAC2 = 22.5 AB. After a visual investigation to discard artefacts and any objects with troubling photometry, we were left with a final sample of 3900 candidates. We retrieved the physical parameter estimates for these objects from the spectral energy distribution-fitting tool `CIGALE`.

Our results confirm that HIERO galaxies can populate the high-mass end of the stellar mass function at $z > 3$, with some sources reaching extreme stellar masses ($M_* > 10^{11} M_\odot$) and exhibiting high dust attenuation values ($A_V > 3$). However, we consider the stellar mass estimates unreliable for sources at $z > 3.5$. For this reason, we favour a more conservative lower-z solution. The challenges faced by spectral energy distribution-fitting tools in accurately characterising these objects underscore the need for further studies that incorporate both observations at shorter wavelengths and spectroscopic data. *Euclid* spectra will help resolve degeneracies and better constrain the physical properties of the brightest galaxies. Given the extreme nature of this population, characterising these sources is crucial for building a comprehensive picture of galaxy evolution and stellar mass assembly across most of the history of the Universe. This work demonstrates *Euclid*'s potential to provide statistical samples of rare objects, such as massive, dust-obscured galaxies at $z > 3$, which will be prime targets for JWST and the Atacama Large Millimeter/submillimeter Array (ALMA).

Key words. methods: observational – techniques: photometric – galaxies: evolution – galaxies: high-redshift – infrared: galaxies

1. Introduction

Understanding the evolution of galaxies throughout cosmic history has always been a fundamental objective of extragalactic astronomy. Observational constraints are crucial for validating theoretical predictions, which must be able to accurately replicate empirical phenomena. A key challenge in this endeavour lies in achieving a complete census of the galaxy population, particularly during the early epochs of the Universe.

The *Hubble* Space Telescope (HST) has been instrumental in the study of high-redshift galaxies, primarily through observations of their rest-frame ultraviolet (UV) emission. These kinds of galaxies have been extensively characterised across the redshift range $3 \lesssim z \lesssim 11$ (Steidel & Hamilton 1993; Steidel et al. 1995; Madau et al. 1996; Steidel et al. 1999; Bouwens et al. 2015; Oesch et al. 2016). However, this UV-based selection systematically misses massive, dusty galaxies, underestimating the true stellar mass function at different epochs (Rodighiero et al. 2007; Wang et al. 2019). Such dust-obscured sources are faint or undetected even in the deepest HST observations, earning them the label HST-dark galaxies or optically dark galaxies (ODGs).

Longer-wavelength facilities such as *Spitzer* and the Atacama Large Millimeter/submillimeter Array (ALMA) have played a crucial role in unveiling this population (Caputi et al. 2015; Franco et al. 2018; Dudzevičiūtė et al. 2020). Recently, the *James Webb* Space Telescope (JWST) has revolutionised the field by providing robust photometric redshifts and stellar mass estimates for these galaxies, thanks to its sensitivity and spatial resolution in the near-infrared (Gardner et al. 2023; Barrufet et al. 2023; Rodighiero et al. 2023). Nonetheless, JWST's relatively narrow field of view limits its capacity for statistical investigations, which are essential for understanding the broader implications of this population on galaxy evolution.

The *Euclid* mission (Laureijs et al. 2012; Euclid Collaboration: Mellier et al. 2025), launched in July 2023 by the European Space Agency (ESA), provides an unparalleled opportunity to address these limitations. Equipped with the Visible Camera (VIS) for optical imaging (Euclid Collaboration: Cropper et al. 2025) and the Near-Infrared Spectrometer and Photometer (NISP) for near-infrared observations (Euclid Collaboration: Schirmer et al. 2023; Euclid Collaboration: Jahnke et al. 2025), *Euclid* is optimised for wide-field surveys, enabling statistical analyses of rare galaxy populations. With its Early Release Observations (EROs; Euclid Early Release Observations 2024), *Euclid* has already demonstrated its potential for identifying massive, dusty galaxies, especially when combined with ancillary data from the *Spitzer*/Infrared Array Camera (IRAC; Girardi et al. 2025).

With the first quick data release (Q1; Euclid Quick Release Q1 2025), we now have access to high-quality observations covering an area of approximately 60 deg^2 area. This study focusses on a specific subset of ODGs known as HST-to-IRAC extremely red objects (HIEROs), identified using the colour criterion $H_E - \mathrm{IRAC2} > 2.25$ (Wang et al. 2016; Caputi et al. 2012). By leveraging the overlap between Euclid Deep Field (EDF) and existing *Spitzer* imaging, we aim to refine the photometric redshifts and stellar mass estimates of this population. We are particularly interested in this population due to its contribution to the high-mass end of the stellar mass function at $z \gtrsim 4$ (Barrufet et al. 2023; Rodighiero et al. 2023; Wang et al. 2025; Traina et al. 2024; Rodighiero et al. 2007; Gottumukkala et al. 2024).

The paper is structured as follows: In Sect. 2 we describe the *Euclid* data products and the creation of the *Spitzer*/IRAC photometric catalogue. In Sect. 3 we explain the selection of our sample and the methodology used to derive their physical properties. Lastly, in Sect. 4 we present our statistical analysis and discuss the results.

Throughout this work, we adopt a Λ cold dark matter (CDM) cosmology with parameters from Planck Collaboration et al. (2016) and a Chabrier (2003) initial mass function (IMF). All magnitudes are reported in the AB system.

⋆ e-mail: `giorgia.girardi.1@phd.unipd.it`

2. Data description

2.1. Euclid catalogues

We exploited the official catalogues released inside the Euclid Consortium for Q1. The detailed description of the data can be found in Euclid Collaboration: Aussel et al. (2025), Euclid Collaboration: McCracken et al. (2025), Euclid Collaboration: Polenta et al. (2025), and Euclid Collaboration: Romelli et al. (2025).

In summary, Q1 extragalactic observations cover 63 deg^2 across three fields: the Euclid Deep Field Fornax (EDF-F), covering 12 deg^2; the Euclid Deep Field North (EDF-N), with 22 deg^2; and the Euclid Deep Field South (EDF-S), with 28 deg^2. All the fields have been observed in the four *Euclid* bands, covering from the visible (I_E, Euclid Collaboration: Cropper et al. 2025) to the near-infrared (NISP, Y_E, J_E, and H_E band; see Euclid Collaboration: Jahnke et al. 2025). These space-based observations are further supplemented by ground-based data collected with different instruments, covering wavelengths from 0.3 µm to 0.9 µm. The ground-based data are included in the officially released dataset as part of the Ultraviolet Near-Infrared Optical Northern Survey (UNIONS, Gwyn et al. 2025) or the Dark Energy Survey (Abbott et al. 2018). The available bands are reported in Table 1.

2.2. Spitzer/IRAC photometry

We analysed IRAC images[1] described in Euclid Collaboration: Moneti et al. (2022). These observations partially overlap with the EDFs and are part of the Cosmic Dawn survey (Euclid Collaboration: McPartland et al. 2025). It is worth noting that the images do not have uniform coverage, both in area and depth, since they were collected by different programmes.

For consistency, we adopted the same IRAC photometry included in the pipeline used to derive the physical parameters for the *Euclid* sources (Euclid Collaboration: Enia et al. 2025). We exploited the two available IRAC bands at 3.6 µm (IRAC1) and 4.5 µm (IRAC2). In this work we did not consider the photometry at 5.8 µm (IRAC3) and 8.0 µm (IRAC4), since that is much shallower and inhomogeneous with respect to the other bands (see Table 1).

While more details on the IRAC photometry measurements can be found in Euclid Collaboration: Bisigello et al. (2025), in the following we briefly summarise the methodology. Using the `photutils` Python package (Bradley et al. 2024), we subtracted the background from each image by calculating the median with a 3×3 pixel filter. Again with `photutils`, aperture photometry was then performed on the IRAC images, forcing the detection to the *Euclid* source positions and using a 1″ radius aperture. This choice excludes any source that would be detectable by IRAC but not by the *Euclid* bands.

However, due to the different point spread functions (PSFs) of the two instruments, which cause significant source blending in the IRAC images, and in line with our goal of obtaining a reliable rather than a complete sample, we chose not to include in this study objects presenting blending or contamination effects. When available, future works will exploit the official *Euclid* catalogue where the de-blending has been performed on the *Spitzer* images.

For EDF-N, we conducted a separate extraction using co-added IRAC1 and IRAC2 *Spitzer* images, weighted by uncertainty maps, and measured fluxes within Kron apertures (Graham & Driver 2005). We applied a Kron scaling factor of 1.8 and a minimum unscaled radius of 2.5 pixels. Aperture and Kron fluxes from the separate extractions were compared to derive aperture-to-total corrections, which were uniformly applied to all filters. The final fluxes are consistent with the catalogues described in Euclid Collaboration: Zalesky et al. (2025), which cover two of the three EDFs.

[1] Retrieved at this page: https://exchg.calet.org/Spitzer/linear/

Table 1. All the available bands in the Q1 data release, differentiated by the three fields.

Band	$\lambda_{\rm eff}$ [µm]	EDF-F	EDF-N	EDF-S
CFHT/MegaCam *u*	0.372	...	23.5	...
HSC *g*	0.480	...	25.3	...
CFHT/MegaCam *r*	0.640	...	24.1	...
PAN-STARRS *i*	0.755	...	23.3	...
HSC *z*	0.891	...	23.5	...
Decam *g*	0.473	24.6	...	24.6
Decam *r*	0.642	24.3	...	24.3
Decam *i*	0.784	23.7	...	23.7
Decam *z*	0.926	22.9	...	22.9
VIS I_E	0.715	24.7	24.7	24.7
NISP Y_E	1.085	23.1	23.1	23.1
NISP J_E	1.375	23.2	23.2	23.2
NISP H_E	1.773	23.2	23.2	23.2
IRAC [IRAC1]	3.550	24.0	24.0	23.1
IRAC [IRAC2]	4.493	23.9	23.9	23.0
IRAC [IRAC3]	5.696	21.2	20.0	...
IRAC [IRAC4]	7.799	19.9	21.1	...

Notes. The reported magnitudes are the $10\,\sigma$ observed depths. Optical and *Euclid* magnitudes refer to an extended source in an aperture diameter of twice the FWHM (Euclid Collaboration: Romelli et al. 2025). IRAC1 and IRAC2 depths correspond to average values in the fields derived considering 2″ empty apertures (more details available in Euclid Collaboration: Moneti et al. 2022 and Euclid Collaboration: McPartland et al. 2025). For IRAC3 and IRAC4 we report the depth derived from the IRAC catalogue, after correcting from aperture magnitude to total magnitude.

3. Methods

3.1. HIERO sample selection

We produced a merged *Euclid* + *Spitzer* catalogue by matching the IDs of the sources, given the application of the photometry performed on the *Spitzer* images at the *Euclid* positions. The available bands and the respective observed depths are reported in Table 1.

To ensure the robustness of our sample, before applying our colour selection, we implemented a series of cuts:

1. `SPURIOUS_FLAG` = 0;
2. `DET_QUALITY_FLAG` < 4;
3. `MUMAX_MINUS_MAG` > −2.6;
4. $23.9 - 2.5\ \log_{10}$(`FLUX_H_TOTAL`) < 24.5;
5. `flag_H` = 0.

The first cut ensures the removal of all the objects that have been labelled as spurious in the official catalogue. Similarly, the second flag requires that the photometry is good, and the fourth one requires a magnitude below 24.5 in the H_E band. The decision to apply a magnitude cut in the H_E band is due to the fact that this is one of the two bands used in our colour selection

Table 2. Total number of objects in the merged *Euclid* + *Spitzer* catalogue and the remaining number of objects after each cleaning step, shown for the three fields.

Field	Fornax	North	South
Original sample	5 328 489	11 378 352	13 060 965
Clean sample	2 837 465	5 365 713	6 534 328
HIERO sample	5263	8258	13 385
Final HIERO sample	920	1051	1899

Notes. The clean sample is the result after applying the cuts described in Sect. 3. The HIERO sample is obtained by applying the colour criterion $H_E - \mathrm{IRAC2} > 2.25$ in the clean sample. Lastly, the final HIERO sample is the result of our visual check (see Sect. 3.2).

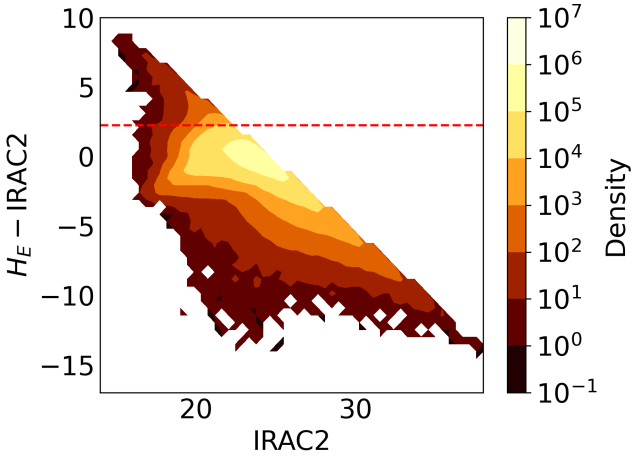

Fig. 1. Colour-magnitude plot of the clean sample. All the objects above the red line, representing $H_E - \mathrm{IRAC2} > 2.25$, i.e. the HIERO colour selection (Wang et al. 2016), are included in our HIERO sample. The diagonal cut is due to the magnitude limit in the H_E band.

(see the next paragraph). This is a conservative choice, in order to deal only with the brightest and most massive sources. The `MUMAX_MINUS_MAG` quantity, instead, represents a sort of estimate of the compactness of the sources, and this cut should remove all the stars present in the catalogue. In fact, `MU_MAX` is the peak surface brightness above the background; thus, the estimator `MUMAX_MINUS_MAG` is related to the concentration of light at the peak versus the total magnitude (Euclid Collaboration: Romelli et al. 2025; Euclid Collaboration: Tucci et al. 2025). The last condition ensures that the H_E band is not affected by spurious detections or artefacts. Again, we decided to include it given that our selection mainly relies on this band. We show in Table 2 the initial number of objects and the resulting number after applying these cuts.

To this clean catalogue, we applied the colour selection that identifies HIERO objects, as defined by Wang et al. (2016), and originally introduced by Caputi et al. (2012): $H_E - \mathrm{IRAC2} > 2.25$. This colour selection is optimised to identify galaxies with $A_V \gtrsim 2$ mag and $\log_{10}(M_*/M_\odot) \approx 10$ at $z \gtrsim 3$ (Gottumukkala et al. 2024). Figure 1 shows the entire clean parent sample, with the red line marking the $H_E - \mathrm{IRAC2} = 2.25$ limit to our selection. All the objects falling above this line respect the HIERO definition. Out of the 14 737 506 objects in the clean sample, 26 906 candidates respect the colour criterion imposed and end up in our HIERO sample.

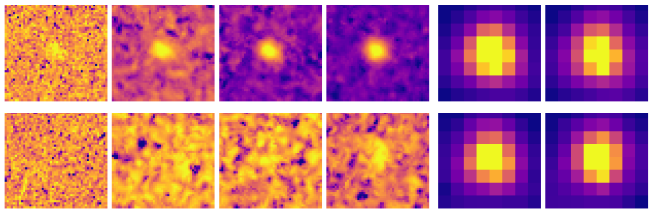

Fig. 2. Examples of two HIEROs that passed our visual check and that were kept in our final catalogue. From left to right: I_E, Y_E, J_E, H_E, IRAC1, and IRAC2. Each cutout has a size of 5″ × 5″.

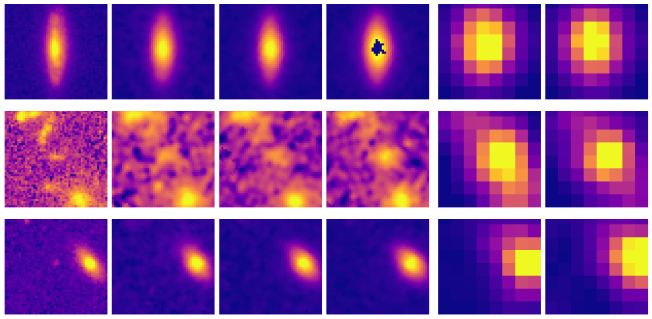

Fig. 3. Examples of three HIEROs that did not pass our visual check and were discarded from our final catalogue. From left to right: I_E, Y_E, J_E, H_E, IRAC1, and IRAC2. Each cutout has a size of 5″ × 5″.

3.2. Visual investigation of the candidate HIEROs

To maximise the reliability of the sources in our sample, we performed a visual check of all the HIERO selected according to the colour criterion presented in Fig. 1. This is mandatory to account for various issues that could affect these data and in order to provide the most conservative sample for the statistical purposes of this paper. We prioritised the purity at the expense of the completeness. As reported in Sect. 3.1, for a total of 26 906 objects we created a set of postage stamps, including the four *Euclid* bands and the first two IRAC channels with a size of 5″ × 5″.

Some examples of good, isolated objects are reported in Fig. 2. We also highlight how the applied colour selection naturally includes dropout objects (bottom panel of Fig. 2). The difference in the PSFs of *Euclid* and *Spitzer* – with full widths a half maximum (FWHMs) of the order of 1.″5 in the first two IRAC channels – is evident from the images. This immediately leads to a large uncertainty in the physical association of objects detected with the two instruments. In particular, blending of *Euclid* sources in the IRAC images is a major issue. Figure 3 shows some such cases (middle panel), together with other examples of HIERO candidates that we decided to discard. For example, automatic masking of pixels from the *Euclid* pipeline can bias the measured fluxes in some bands, leading to artificially red galaxies (top panel). This does not imply that the object is not a valid candidate; rather, the available *Euclid* photometry is insufficient to accurately recover its true colours. An alternative approach would have been to mask the same pixels across all bands. However, given our goal of constructing a conservative and robust sample, we opted to discard such objects instead. Furthermore, the adopted IRAC photometry (see Sect. 2.2), extracted at the position of the *Euclid* sources, leads to cases where the corresponding IRAC flux is emitted by a different *Spitzer* object (bottom panel in Fig. 3, where a faint VIS detection is visible at the centre of the cutout). We further discarded sources falling at the edges of the maps or dominated by any other evident artefacts.

Table 3. Input models and main parameters for the CIGALE code.

`sfh_delayed`	
τ (main) [Myr]	200, 300, 500, 700 1000, 1500, 2000
Age (main) [Myr]	200, 300, 500, 700 1000, 1500, 5000
`bc03`	
IMF	Chabrier
Metallicity	0.008, 0.02
`nebular`	
logU	$-4.0, -3.0, -2.0, -1.0$
Emission	True
`dustatt_modified_starburst`	
E_{BV} lines [mag]	$0, 0.1, \ldots, 4.4, 4.5$
E_{BV} factor	0.44
R_V	3.1
`redshifting`	
Redshift	$0, 0.1, \ldots, 14.9, 15$

Notes. The models used are: a delayed star-formation history with optional exponential burst; Bruzual & Charlot (2003) simple stellar population model; a continuum and line nebular emission model; a modified Calzetti et al. (2000) dust attenuation law; and a redshifting model that also includes the intergalactic medium from Meiksin (2006).

To summarise, we determined whether to discard an object based on the following criteria:

1. the presence of bad pixels invalidating the photometry;
2. the presence of other *Euclid* sources within the IRAC FWHM;
3. flux in the IRAC bands contaminated by nearby sources.

Our conservative approach leads to a significant reduction in the number of HIERO sources retained in this study, with only 15% surviving the selection process. The exact values for each deep field are provided in Table 2, resulting in a final sample of 3870 sources. While we acknowledge that discarding such a large number of objects is not ideal, the primary goal of this first work is to ensure a highly conservative selection. Consequently, we did not use this sample for statistical analyses, such as computing the stellar mass function, since completeness cannot be reliably reproduced. These analyses will be conducted once deblended IRAC photometry becomes available for all three EDFs.

3.3. Physical parameter retrieval

In this study we exploited the Python code CIGALE (Boquien et al. 2019), given its fast response. We considered detections only the fluxes presenting S/N > 3, for all the others we set the flux to 0 and the error as 3 times the observed depth reported in Table 1. The setup is reported in Table 3.

We mimicked the setup used in the analogous work with the ERO data (Girardi et al. 2025). The A_V value is up to 6, since we expect very dusty sources; while the redshift is free to go up to 15. This is because we expect both low- and high-z contaminants. With the wide nebular parameter range we ensure that we are not overestimating the mass due to mistaking the emission lines as the continuum, given the absence of data at longer wavelengths that could mitigate this problem. This could lead to an overestimation by up to a factor of 10 (Bisigello et al. 2019; Papovich et al. 2023; Wang et al. 2025).

4. Results and discussion

Given the significant uncertainties and degeneracies associated with photometric redshift estimation, we focussed on sources with at least three detections. When only one or two photometric points are available, even when considering upper limits, the fits cannot be considered reliable. Despite this restriction, the large sample size still enables a meaningful analysis. Prioritising robustness over completeness, we exclude these sources from further discussion. The resulting final sample consists of 2994 galaxies.

4.1. Constraints on the number density

While the primary focus of this work is the construction of a robust, clean sample, we also provide an approximate estimate of their number density, statistically accounting for sources of incompleteness and contamination, particularly those related to IRAC photometry.

A major challenge in selecting red sources like HIEROs arises from source blending in IRAC imaging, due to the large PSF. To mitigate this, we visually inspected all candidates and retained only those that appear isolated and uncontaminated in both the $H_{\rm E}$ band and IRAC2 images (see Sect. 3.2). As a result, our final clean sample consists exclusively of visually confirmed isolated sources, ensuring that their IRAC photometry is reliable. However, this strict isolation criterion inevitably introduces incompleteness by systematically excluding genuine HIEROs that lie close to other sources and whose photometry is therefore blended.

To account for this, we applied a statistical correction inspired by the method used in Wang et al. (2019). Rather than applying an additional isolation cut, we used the fact that our sample already consists of isolated sources to estimate the fraction of HIEROs that would be missed due to blending. Specifically, we computed the probability that a genuine source would appear isolated within a radius of 2″, given the number density of *Euclid* sources.

From the reliable *Euclid* sample, we find a surface number density of $N \sim 0.026$ arcsec^{-2}. Under the assumption of a random spatial distribution, the probability that a galaxy has no neighbours within a radius r is $p = \exp(-N\pi r^2)$. For $r = 2''$, this yields $p = 0.72$, corresponding to a correction of approximately 28%. This correction could be underestimated, given that previous studies have found that HIEROs tend to be massive galaxies; therefore, they are expected to preferentially be in over-dense environments. Consequently, despite the reliability of our selection, a significant fraction of true HIEROs are likely excluded due to random superpositions with nearby sources, and this effect must be taken into consideration. Regarding the IRAC2 depth, a completeness correction should be negligible, as all sources lie above the $10\,\sigma$ observed depth reported in Table 1.

Although future improvements in de-blending techniques will enhance the accuracy of IRAC photometry, such methods may still struggle with very close source pairs. This approach, based on a statistical treatment of incompleteness, provides a conservative yet meaningful constraint on the true number density of such massive, red galaxies.

With this corrected estimate, it is instructive to compare our results with those found in the literature. We limited the comparison to studies where the applied selection is closely aligned with ours. In particular, we report the number densities (calculated as number counts divided by the area) from Wang et al. (2016),

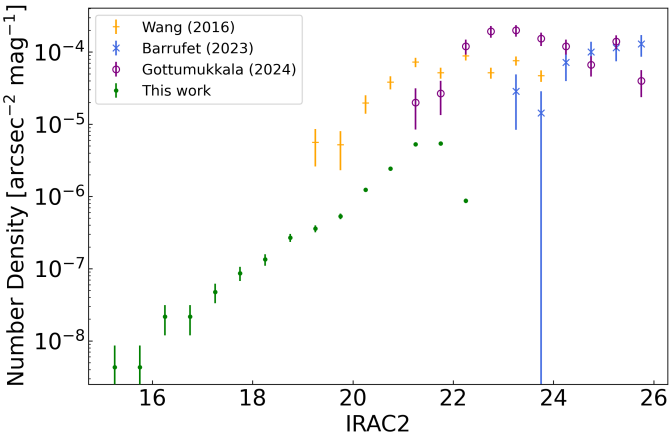

Fig. 4. Number counts normalised by area as a function of IRAC2 magnitude. Different colours and symbols represent results from different studies.

where the selection was first introduced, as well as from Barrufet et al. (2023) and Gottumukkala et al. (2024), who used the colour criteria $F160W - F444W > 2.0$ and $F150W - F444W > 2.1$, respectively.

As shown in Fig. 4, the different estimates do not always agree. As expected, JWST is able to probe much fainter 4.4 µm magnitudes. It is worth noting that the error bars on the y axis, which is plotted on a logarithmic scale, are computed assuming Poissonian noise. We did not consider other source of errors, so the true uncertainties may be underestimated. Small differences in the selection criteria also contribute to the lack of full agreement between the estimates.

Our values typically lie about one order of magnitude below those reported by Wang et al. (2016), while they appear more consistent with Gottumukkala et al. (2024) in the overlapping magnitude bins. A direct comparison, however, is challenging due to the different cleaning procedures applied to the samples in the cited studies. As expected, we have prioritised reliability over completeness; therefore, even after applying the statistical correction, our number densities are likely to be underestimated. For instance, during the visual inspection (see Sect. 3.2), we discarded numerous objects affected by defects or masks in the *Euclid* images. Although these candidates could be genuine HIEROs, they did not satisfy the requirements of our final selection criteria.

Another important consideration is that, by construction, our sample excludes the H_E-undetected sources (see Sect. 2.2), which are included in the samples of the other studies. For instance, in the sample presented by Wang et al. (2016), H_E-undetected objects constitute approximately 6.3% of the total. In our case, this fraction would likely be even higher due to the shallower data. This limitation will be addressed in future work, which will take advantage of the de-blended *Spitzer*/IRAC catalogues available for the EDFs. Nevertheless, this plot highlights the true power of *Euclid*: thanks to its unmatched field of view, we are able recover IRAC2 magnitudes up to 15 mag, extending our current knowledge towards the bright end.

4.2. Derived galaxy properties

Despite removing sources with the fewest photometric detections, we stress that a fraction of our sample still relies on spectral energy distribution (SED) fits constrained by only three or four detections with S/N > 3. Given these limitations, we invite the reader to interpret the derived photometric redshifts and galaxy properties with caution. This uncertainty is reflected in the non-negligible errors, reported in each plot. Future observations of the EDFs will be crucial for these objects, because they will benefit from the increased depth of upcoming surveys.

We first present the M_* versus z distribution in Fig. 5. The left panel displays all data points for sources with three or more detections, using values derived from `CIGALE`. The grey-shaded region represents the prohibited area according to the ΛCDM cosmological model, where baryonic conversion efficiency (ϵ) exceeds 100%. Approximately 9.7% of the sample falls within this region. The vertical dotted red line marks $z = 3.5$, with sources to the right of this line represented by red dots; we refer to these as high-z sources from this point onwards. Given the limited photometric information and the relatively shallow depth of this data release (as reported in Table 1), we do not place full confidence in the SED-fitting results for these objects.

We also took into account the findings of Forrest et al. (2024), whose empirical study suggests that SED-fitting estimates yielding $M_* > 10^{11.7}\,M_\odot$ at $3 < z_{\rm phot} < 4$ are not supported by spectroscopic observations. Specifically, they selected a sample of red objects with such estimated properties and obtained spectroscopic data. Upon comparison, none of the objects satisfied $z_{\rm spec} - z_{\rm phot} < 0.5$, underscoring the difficulty in accurately characterising such sources. Their results, based on very high S/N observations and a broader set of observed bands, rely on more robust photometry. Given this distinction, we opted not to impose a stellar mass cut but instead to focus solely on redshift considerations.

This decision is further supported by an analysis of the total redshift distribution of the EDFs, normalised by total counts and shown in Fig. 6. We find that our number counts at $z > 3.5$ exceed those reported by Gottumukkala et al. (2024) in the Cosmic Evolution Early Release Science (CEERS) field. This mismatch is more clearly quantified by comparing the median redshift values. In fact, we find $z_{\rm median} = 3.79$, whereas their analysis reports $z_{\rm median} = 3.13$. The latter study utilises JWST observations covering a significantly smaller area (about 80 arcmin^2) but reaching considerably greater depth than the current Q1 data release. This discrepancy raises concerns about the reliability of our photometric redshift estimates for the high-z sub-sample. To address this, we performed a second `CIGALE` run, constraining the redshift to $z < 3.5$. The right panel of Fig. 5 presents the same distribution, but incorporates the results from this second run for high-z sources, which are still shown as red dots to illustrate their redistribution. We observe that these empirical constraints align well with the theoretical limit, reducing the fraction of points in the prohibited area to approximately 0.17%. Given this refined distribution, we did not blindly trust the SED-fitting tool's results, but instead integrated both empirical and theoretical insights.

Preferring a lower-z solution for this sub-sample implies prioritising a low-z interpretation over a high-z one. In fact, in the preliminary work of Girardi et al. (in prep.), we found that nearly all HIEROs exhibit a bimodal or multi-peak probability distribution function for redshift. This is due to the degeneracy between a high-z, less dusty solution and a lower-z, dustier one. Statistically, some objects are likely to be genuine high-z sources; however, given our inability to discern which cases reflect true high-z objects versus those with overestimated photometric redshifts, we adopted a conservative approach. The presence of high-z sources could be further tested in a future work with longer wavelength data, such as sub-millimetre observations from *Herschel*/SPIRE. Based on all these considerations, we proceed by

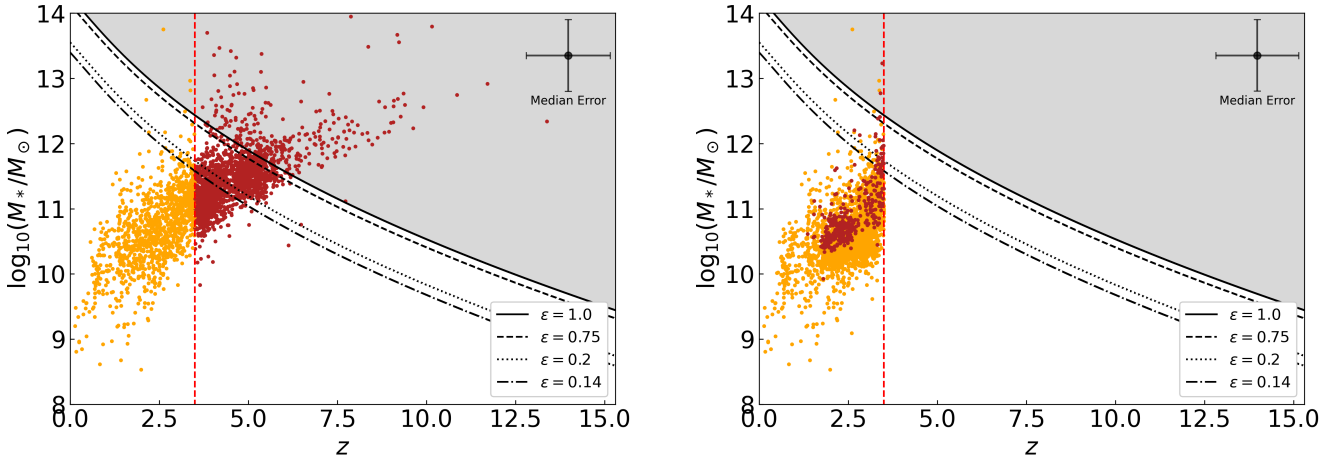

Fig. 5. Stellar mass versus redshift distribution of the HIERO sample. The y-axis is on a logarithmic scale. The vertical dotted red line corresponds to $z = 3.5$, above which we do not trust the solutions found by the fit. These high-z sources are displayed as red dots. The grey-shaded area represents the region forbidden by the ΛCDM model. The black lines show the limit for different values of ϵ. The median error for both the quantities is reported in the top-right corner of the plot. Left panel: Results from the CIGALE run described in Sect. 3.3. Right panel: Results from the low-z run for the high-z objects, which are still displayed as red dots.

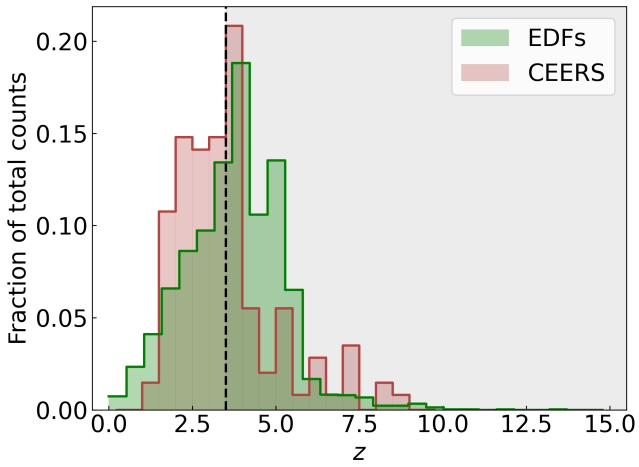

Fig. 6. Redshift distributions for the total HIERO sample in the EDFs (green) compared to the distribution found by Gottumukkala et al. (2024) in the CEERS field applying a similar selection, (red). The vertical line corresponds to $z = 3.5$.

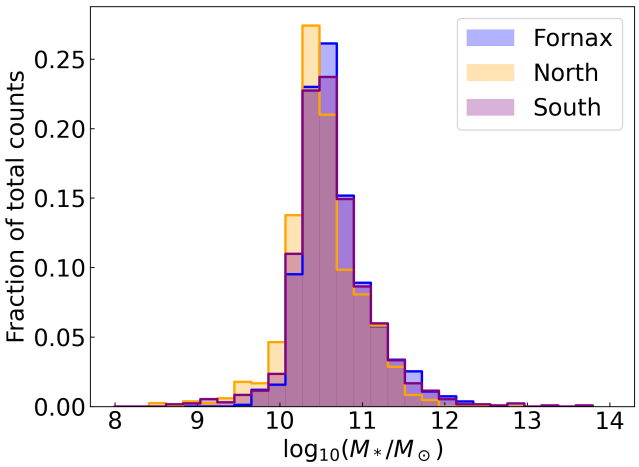

Fig. 7. Stellar mass distributions for EDF-F (blue), EDF-N (orange), and EDF-S (purple). The counts of the distributions are normalised to the total number of objects in each field.

presenting and discussing results derived from the distribution shown in the right panel of Fig. 5.

Figure 7 shows the distribution of the stellar masses. The counts are proportional to the different numbers of candidates in the different fields. We find a mean value of $\langle M_* \rangle = 10^{10.6}\, M_\odot$, a value that confirms the expected massive nature of these sources.

Studying this type of source, we are interested in looking at the dust attenuation values since we expect them to be very dusty. We find a mean value of $\langle A_V \rangle = 2.3$, confirming the expectation. Looking at the A_V versus M_* distribution, shown in Fig. 8, we see that our points are spread across quite a broad range, covering A_V from about 0 up to 6. For reference, the expected relation for normal galaxies in McLure et al. (2018) is also shown as a solid dark teal line. Our sample roughly follows this relation, revealing, however, a possible population of extremely obscured objects at $M_* > 10^{10}\, M_\odot$. This proves the power of *Euclid* in providing statistical samples of candidates of such rare objects for subsequent follow-up observations using other facilities, in order to confirm their redshifts and nature. For comparison, we include in this plot recent results from the literature of samples selected with similar criteria (Pampliega et al. 2019; Pérez-González et al. 2023; Gentile et al. 2024), including much fainter JWST dark objects.

5. Conclusions

In this study we exploited the Q1 *Euclid* data release to characterise HIERO galaxies, a dusty and massive population exhibiting extremely red colours. Starting from the official *Euclid* photometric catalogue, we applied a series of selection cuts (see Sect. 3.1) to isolate candidates that meet the HIERO colour criteria. This process resulted in a clean sample of 26 906 sources.

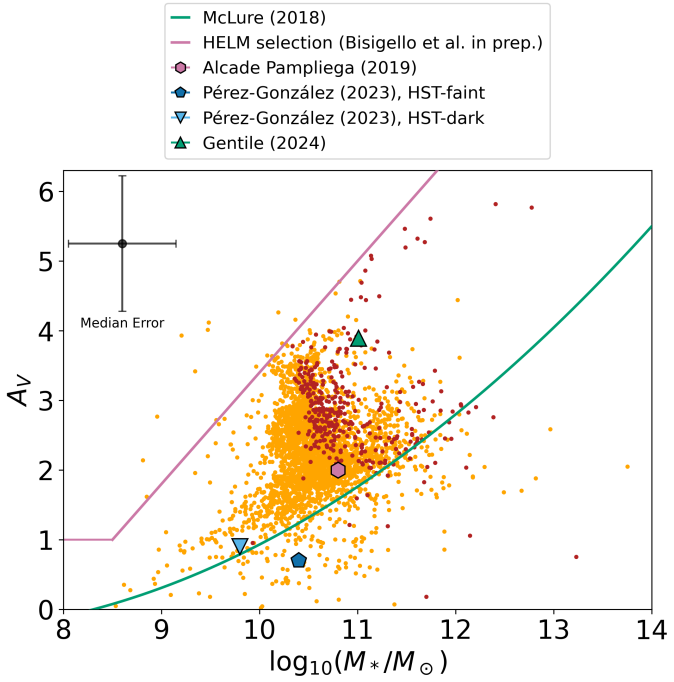

Fig. 8. Dust attenuation versus stellar mass of the HIERO sample. The x-axis is on a logarithmic scale. The solid dark teal line reports the relation from McLure et al. (2018), while the purple line delimits the area that identifies the so-called Highly Extincted Low-Mass (HELM) galaxies (Bisigello et al. 2025). The median error for both quantities is reported in the top-left corner of the plot. Different symbols report values from previous studies, as indicated in the legend.

To ensure the robustness of our sample, we performed a rigorous visual inspection, retaining only candidates with reliable photometry (i.e. free from defects, masked regions, or blending or contamination issues in the IRAC bands; see Sect. 3.2). This refinement led to a final sample of 3870 sources.

We used an SED-fitting code to derive the physical properties of these objects (see Sect. 3.3). To enhance the robustness of our sample, we included only sources with at least three photometric detections (S/N > 3). However, the results should be interpreted with caution as in some cases the SED fitting relies on only three or four photometric points. Nevertheless, we believe these findings are valuable, both for anticipating the potential of future *Euclid* data releases and as a foundation for further investigations.

The wide area of the EDFs enabled us to obtain meaningful statistics, even after applying all the selection cuts to define the final sample. This is particularly crucial for these rare objects, which would otherwise be challenging to characterise. The next step is to leverage future data releases to accurately determine the HIERO contribution to the stellar mass function across different epochs, a task that will be addressed in a forthcoming paper.

This pilot analysis highlights the need for further studies to fully understand this population. Our results show that these objects span a broad range of parameters, leaving their nature uncertain. Obtaining spectroscopic data will be crucial to better constraining their properties. *Euclid*'s slitless spectroscopy will help disentangle the degeneracy between redshift and dust attenuation and in turn help determine whether the identified high-z contaminants are genuine or instead represent more dust-obscured sources at lower redshifts.

Overall, *Euclid* has demonstrated its potential as a pivotal instrument for studying this massive and dusty population. Even more exciting results are expected with the DR1 *Euclid* data release, which will cover approximately 1900 deg^2 of sky.

Acknowledgements. The research activities described in this paper were carried out with contribution of the Next Generation EU funds within the National Recovery and Resilience Plan (PNRR), Mission 4–Education and Research, Component 2–From Research to Business (M4C2), Investment Line 3.1–Strengthening and creation of Research Infrastructures, Project IR0000034–"STILES–Strengthening the Italian Leadership in ELT and SKA". This work has made use of the *Euclid* Quick Release Q1 data from the *Euclid* mission of the European Space Agency (ESA), 2025, https://doi.org/10.57780/esa-2853f3b. The Euclid Consortium acknowledges the European Space Agency and a number of agencies and institutes that have supported the development of *Euclid*, in particular the Agenzia Spaziale Italiana, the Austrian Forschungsförderungsgesellschaft funded through BMK, the Belgian Science Policy, the Canadian Euclid Consortium, the Deutsches Zentrum für Luft- und Raumfahrt, the DTU Space and the Niels Bohr Institute in Denmark, the French Centre National d'Etudes Spatiales, the Fundação para a Ciência e a Tecnologia, the Hungarian Academy of Sciences, the Ministerio de Ciencia, Innovación y Universidades, the National Aeronautics and Space Administration, the National Astronomical Observatory of Japan, the Netherlandse Onderzoekschool Voor Astronomie, the Norwegian Space Agency, the Research Council of Finland, the Romanian Space Agency, the State Secretariat for Education, Research, and Innovation (SERI) at the Swiss Space Office (SSO), and the United Kingdom Space Agency. A complete and detailed list is available on the *Euclid* web site (www.euclid-ec.org). This research makes use of ESA Datalabs (datalabs.esa.int), an initiative by ESA's Data Science and Archives Division in the Science and Operations Department, Directorate of Science.

References

Abbott, T. M. C., Abdalla, F. B., Allam, S., et al. 2018, ApJS, 239, 18
Barrufet, L., Oesch, P., Weibel, A., et al. 2023, MNRAS, 522, 449
Bisigello, L., Caputi, K., Colina, L., et al. 2019, ApJ, 243, 27
Bisigello, L., Gandolfi, G., Feltre, A., et al. 2025, A&A, 693, L18
Boquien, M., Burgarella, D., Roehlly, Y., et al. 2019, A&A, 622, A103
Bouwens, R. J., Illingworth, G., Oesch, P., et al. 2015, ApJ, 803, 34
Bradley, L., Sipőcz, B., Robitaille, T., et al. 2024, astropy/photutils: 1.12.0
Bruzual, G. & Charlot, S. 2003, MNRAS, 344, 1000
Calzetti, D., Armus, L., Bohlin, R. C., et al. 2000, ApJ, 533, 682
Caputi, K., Ilbert, O., Laigle, C., et al. 2015, ApJ, 810, 73
Caputi, K. I., Dunlop, J. S., McLure, R. J., et al. 2012, ApJ, 750, L20
Chabrier, G. 2003, PASP, 115, 763
Dudzevičiūtė, U., Smail, I., Swinbank, A., et al. 2020, MNRAS, 494, 3828
Euclid Collaboration: Aussel, H., Tereno, I., Schirmer, M., et al. 2025, A&A, submitted (Euclid Q1 SI), arXiv:2503.15302
Euclid Collaboration: Bisigello, L., Rodighiero, G., Fotopoulou, S., et al. 2025, A&A, in press (Euclid Q1 SI), https://doi.org/10.1051/0004-6361/202554537, arXiv:2503.15323
Euclid Collaboration: Cropper, M., Al-Bahlawan, A., Amiaux, J., et al. 2025, A&A, 697, A2
Euclid Collaboration: Enia, A., Pozzetti, L., Bolzonella, M., et al. 2025, A&A, in press (Euclid Q1 SI), https://doi.org/10.1051/0004-6361/202554576, arXiv:2503.15314
Euclid Collaboration: Jahnke, K., Gillard, W., Schirmer, M., et al. 2025, A&A, 697, A3
Euclid Collaboration: McCracken, H. J., Benson, K., Dolding, C., et al. 2025, A&A, in press (Euclid Q1 SI), https://doi.org/10.1051/0004-6361/202554594, arXiv:2503.15303
Euclid Collaboration: McPartland, C. J. R., Zalesky, L., Weaver, J. R., et al. 2025, A&A, 695, A259
Euclid Collaboration: Mellier, Y., Abdurro'uf, Acevedo Barroso, J., et al. 2025, A&A, 697, A1
Euclid Collaboration: Moneti, A., McCracken, H. J., Shuntov, M., et al. 2022, A&A, 658, A126
Euclid Collaboration: Polenta, G., Frailis, M., Alavi, A., et al. 2025, A&A, in press (Euclid Q1 SI), https://doi.org/10.1051/0004-6361/202554657, arXiv:2503.15304
Euclid Collaboration: Romelli, E., Kümmel, M., Dole, H., et al. 2025, A&A, in press (Euclid Q1 SI), https://doi.org/10.1051/0004-6361/202554586, arXiv:2503.15305
Euclid Collaboration: Schirmer, M., Thürmer, K., Bras, B., et al. 2023, A&A, 675, A142

Euclid Collaboration: Tucci, M., Paltani, S., Hartley, W. G., et al. 2025, A&A, in press (Euclid Q1 SI), https://doi.org/10.1051/0004-6361/202554588, arXiv:2503.15306
Euclid Collaboration: Zalesky, L., McPartland, C. J. R., Weaver, J. R., et al. 2025, A&A, 695, A229
Euclid Early Release Observations. 2024, https://doi.org/10.57780/esa-qmocze3
Euclid Quick Release Q1. 2025, https://doi.org/10.57780/esa-2853f3b
Forrest, B., Cooper, M. C., Muzzin, A., et al. 2024, ApJ, 977, 51
Franco, M., Elbaz, D., Béthermin, M., et al. 2018, A&A, 620, A152
Gardner, J. P., Mather, J. C., Abbott, R., et al. 2023, PASP, 135, 068001
Gentile, F., Talia, M., Daddi, E., et al. 2024, A&A, 687, A288
Girardi, G., Grazian, A., Rodighiero, G., et al. 2025, A&A, submitted
Gottumukkala, R., Barrufet, L., Oesch, P., et al. 2024, MNRAS, 530, 966
Graham, A. W. & Driver, S. P. 2005, PASA, 22, 118
Gwyn, S., McConnachie, A. W., Cuillandre, J.-C., et al. 2025, arXiv e-prints, arXiv:2503.13783
Laureijs, R., Gondoin, P., Duvet, L., et al. 2012, in Society of Photo-Optical Instrumentation Engineers (SPIE) Conference Series, Vol. 8442, Space Telescopes and Instrumentation 2012: Optical, Infrared, and Millimeter Wave, ed. M. C. Clampin, G. G. Fazio, H. A. MacEwen, & J. M. Oschmann, Jr., 84420T
Madau, P., Ferguson, H. C., Dickinson, M. E., et al. 1996, MNRAS, 283, 1388
McLure, R., Dunlop, J., Cullen, F., et al. 2018, MNRAS, 476, 3991
Meiksin, A. 2006, MNRAS, 365, 807
Oesch, P. A., Brammer, G., van Dokkum, P. G., et al. 2016, ApJ, 819, 129
Pampliega, B. A., Pérez-González, P. G., Barro, G., et al. 2019, ApJ, 876, 135
Papovich, C., Cole, J. W., Yang, G., et al. 2023, ApJL, 949, L18
Pérez-González, P. G., Barro, G., Annunziatella, M., et al. 2023, ApJL, 946, L16
Planck Collaboration, Ade, P. A. R., Aghanim, N., et al. 2016, A&A, 594, A24
Rodighiero, G., Bisigello, L., Iani, E., et al. 2023, MNRAS Lett., 518, L19
Rodighiero, G., Cimatti, A., Franceschini, A., et al. 2007, A&A, 470, 21
Steidel, C. C., Adelberger, K. L., Giavalisco, M., Dickinson, M., & Pettini, M. 1999, ApJ, 519, 1
Steidel, C. C. & Hamilton, D. 1993, AJ, 105, 2017
Steidel, C. C., Pettini, M., & Hamilton, D. 1995, AJ, 110, 2519
Traina, A., Gruppioni, C., Delvecchio, I., et al. 2024, A&A, 681, A118
Wang, T., Elbaz, D., Schreiber, C., et al. 2016, ApJ, 816, 84
Wang, T., Schreiber, C., Elbaz, D., et al. 2019, Nature, 572, 211
Wang, T., Sun, H., Zhou, L., et al. 2025, ApJ, 988, L35

[1] Dipartimento di Fisica e Astronomia "G. Galilei", Università di Padova, Via Marzolo 8, 35131 Padova, Italy
[2] INAF-Osservatorio Astronomico di Padova, Via dell'Osservatorio 5, 35122 Padova, Italy
[3] Dipartimento di Fisica e Astronomia, Università di Bologna, Via Gobetti 93/2, 40129 Bologna, Italy
[4] INAF-Osservatorio di Astrofisica e Scienza dello Spazio di Bologna, Via Piero Gobetti 93/3, 40129 Bologna, Italy
[5] Jeremiah Horrocks Institute, University of Central Lancashire, Preston, PR1 2HE, UK
[6] Université Paris-Saclay, Université Paris Cité, CEA, CNRS, AIM, 91191, Gif-sur-Yvette, France
[7] School of Physical Sciences, The Open University, Milton Keynes, MK7 6AA, UK
[8] Dipartimento di Fisica e Astronomia "G. Galilei", Università di Padova, Vicolo dell'Osservatorio 3, 35122 Padova, Italy
[9] Institute of Cosmology and Gravitation, University of Portsmouth, Portsmouth PO1 3FX, UK
[10] Kapteyn Astronomical Institute, University of Groningen, PO Box 800, 9700 AV Groningen, The Netherlands
[11] Cosmic Dawn Center (DAWN)
[12] Université Paris-Saclay, CNRS, Institut d'astrophysique spatiale, 91405, Orsay, France
[13] ESAC/ESA, Camino Bajo del Castillo, s/n., Urb. Villafranca del Castillo, 28692 Villanueva de la Cañada, Madrid, Spain
[14] School of Mathematics and Physics, University of Surrey, Guildford, Surrey, GU2 7XH, UK
[15] INAF-Osservatorio Astronomico di Brera, Via Brera 28, 20122 Milano, Italy
[16] IFPU, Institute for Fundamental Physics of the Universe, via Beirut 2, 34151 Trieste, Italy
[17] INAF-Osservatorio Astronomico di Trieste, Via G. B. Tiepolo 11, 34143 Trieste, Italy
[18] INFN, Sezione di Trieste, Via Valerio 2, 34127 Trieste TS, Italy
[19] SISSA, International School for Advanced Studies, Via Bonomea 265, 34136 Trieste TS, Italy
[20] INFN-Sezione di Bologna, Viale Berti Pichat 6/2, 40127 Bologna, Italy
[21] Max Planck Institute for Extraterrestrial Physics, Giessenbachstr. 1, 85748 Garching, Germany
[22] Universitäts-Sternwarte München, Fakultät für Physik, Ludwig-Maximilians-Universität München, Scheinerstrasse 1, 81679 München, Germany
[23] Space Science Data Center, Italian Space Agency, via del Politecnico snc, 00133 Roma, Italy
[24] Dipartimento di Fisica, Università di Genova, Via Dodecaneso 33, 16146, Genova, Italy
[25] INFN-Sezione di Genova, Via Dodecaneso 33, 16146, Genova, Italy
[26] Department of Physics "E. Pancini", University Federico II, Via Cinthia 6, 80126, Napoli, Italy
[27] INAF-Osservatorio Astronomico di Capodimonte, Via Moiariello 16, 80131 Napoli, Italy
[28] Instituto de Astrofísica e Ciências do Espaço, Universidade do Porto, CAUP, Rua das Estrelas, PT4150-762 Porto, Portugal
[29] Faculdade de Ciências da Universidade do Porto, Rua do Campo de Alegre, 4150-007 Porto, Portugal
[30] Dipartimento di Fisica, Università degli Studi di Torino, Via P. Giuria 1, 10125 Torino, Italy
[31] INFN-Sezione di Torino, Via P. Giuria 1, 10125 Torino, Italy
[32] INAF-Osservatorio Astrofisico di Torino, Via Osservatorio 20, 10025 Pino Torinese (TO), Italy
[33] European Space Agency/ESTEC, Keplerlaan 1, 2201 AZ Noordwijk, The Netherlands
[34] Institute Lorentz, Leiden University, Niels Bohrweg 2, 2333 CA Leiden, The Netherlands
[35] Leiden Observatory, Leiden University, Einsteinweg 55, 2333 CC Leiden, The Netherlands
[36] INAF-IASF Milano, Via Alfonso Corti 12, 20133 Milano, Italy
[37] Centro de Investigaciones Energéticas, Medioambientales y Tecnológicas (CIEMAT), Avenida Complutense 40, 28040 Madrid, Spain
[38] Port d'Informació Científica, Campus UAB, C. Albareda s/n, 08193 Bellaterra (Barcelona), Spain
[39] Institute for Theoretical Particle Physics and Cosmology (TTK), RWTH Aachen University, 52056 Aachen, Germany
[40] INAF-Osservatorio Astronomico di Roma, Via Frascati 33, 00078 Monteporzio Catone, Italy
[41] INFN section of Naples, Via Cinthia 6, 80126, Napoli, Italy
[42] Institute for Astronomy, University of Hawaii, 2680 Woodlawn Drive, Honolulu, HI 96822, USA
[43] Dipartimento di Fisica e Astronomia "Augusto Righi" - Alma Mater Studiorum Università di Bologna, Viale Berti Pichat 6/2, 40127 Bologna, Italy
[44] Instituto de Astrofísica de Canarias, Vía Láctea, 38205 La Laguna, Tenerife, Spain
[45] Institute for Astronomy, University of Edinburgh, Royal Observatory, Blackford Hill, Edinburgh EH9 3HJ, UK
[46] Jodrell Bank Centre for Astrophysics, Department of Physics and Astronomy, University of Manchester, Oxford Road, Manchester M13 9PL, UK
[47] European Space Agency/ESRIN, Largo Galileo Galilei 1, 00044 Frascati, Roma, Italy
[48] Université Claude Bernard Lyon 1, CNRS/IN2P3, IP2I Lyon, UMR 5822, Villeurbanne, F-69100, France
[49] Institut de Ciències del Cosmos (ICCUB), Universitat de Barcelona (IEEC-UB), Martí i Franquès 1, 08028 Barcelona, Spain
[50] Institució Catalana de Recerca i Estudis Avançats (ICREA), Passeig de Lluís Companys 23, 08010 Barcelona, Spain
[51] UCB Lyon 1, CNRS/IN2P3, IUF, IP2I Lyon, 4 rue Enrico Fermi, 69622 Villeurbanne, France
[52] Mullard Space Science Laboratory, University College London, Holmbury St Mary, Dorking, Surrey RH5 6NT, UK

[53] Departamento de Física, Faculdade de Ciências, Universidade de Lisboa, Edifício C8, Campo Grande, PT1749-016 Lisboa, Portugal
[54] Instituto de Astrofísica e Ciências do Espaço, Faculdade de Ciências, Universidade de Lisboa, Campo Grande, 1749-016 Lisboa, Portugal
[55] Department of Astronomy, University of Geneva, ch. d'Ecogia 16, 1290 Versoix, Switzerland
[56] INAF-Istituto di Astrofisica e Planetologia Spaziali, via del Fosso del Cavaliere, 100, 00100 Roma, Italy
[57] INFN-Padova, Via Marzolo 8, 35131 Padova, Italy
[58] Aix-Marseille Université, CNRS/IN2P3, CPPM, Marseille, France
[59] INFN-Bologna, Via Irnerio 46, 40126 Bologna, Italy
[60] School of Physics, HH Wills Physics Laboratory, University of Bristol, Tyndall Avenue, Bristol, BS8 1TL, UK
[61] FRACTAL S.L.N.E., calle Tulipán 2, Portal 13 1A, 28231, Las Rozas de Madrid, Spain
[62] NRC Herzberg, 5071 West Saanich Rd, Victoria, BC V9E 2E7, Canada
[63] Institute of Theoretical Astrophysics, University of Oslo, P.O. Box 1029 Blindern, 0315 Oslo, Norway
[64] Jet Propulsion Laboratory, California Institute of Technology, 4800 Oak Grove Drive, Pasadena, CA, 91109, USA
[65] Department of Physics, Lancaster University, Lancaster, LA1 4YB, UK
[66] Felix Hormuth Engineering, Goethestr. 17, 69181 Leimen, Germany
[67] Technical University of Denmark, Elektrovej 327, 2800 Kgs. Lyngby, Denmark
[68] Cosmic Dawn Center (DAWN), Denmark
[69] Institut d'Astrophysique de Paris, UMR 7095, CNRS, and Sorbonne Université, 98 bis boulevard Arago, 75014 Paris, France
[70] Max-Planck-Institut für Astronomie, Königstuhl 17, 69117 Heidelberg, Germany
[71] NASA Goddard Space Flight Center, Greenbelt, MD 20771, USA
[72] Department of Physics and Helsinki Institute of Physics, Gustaf Hällströmin katu 2, 00014 University of Helsinki, Finland
[73] Université de Genève, Département de Physique Théorique and Centre for Astroparticle Physics, 24 quai Ernest-Ansermet, CH-1211 Genève 4, Switzerland
[74] Department of Physics, P.O. Box 64, 00014 University of Helsinki, Finland
[75] Helsinki Institute of Physics, Gustaf Hällströmin katu 2, University of Helsinki, Helsinki, Finland
[76] Centre de Calcul de l'IN2P3/CNRS, 21 avenue Pierre de Coubertin 69627 Villeurbanne Cedex, France
[77] Laboratoire d'etude de l'Univers et des phenomenes eXtremes, Observatoire de Paris, Université PSL, Sorbonne Université, CNRS, 92190 Meudon, France
[78] Aix-Marseille Université, CNRS, CNES, LAM, Marseille, France
[79] SKA Observatory, Jodrell Bank, Lower Withington, Macclesfield, Cheshire SK11 9FT, UK
[80] Dipartimento di Fisica "Aldo Pontremoli", Università degli Studi di Milano, Via Celoria 16, 20133 Milano, Italy
[81] INFN-Sezione di Milano, Via Celoria 16, 20133 Milano, Italy
[82] University of Applied Sciences and Arts of Northwestern Switzerland, School of Computer Science, 5210 Windisch, Switzerland
[83] Universität Bonn, Argelander-Institut für Astronomie, Auf dem Hügel 71, 53121 Bonn, Germany
[84] INFN-Sezione di Roma, Piazzale Aldo Moro, 2 - c/o Dipartimento di Fisica, Edificio G. Marconi, 00185 Roma, Italy
[85] Dipartimento di Fisica e Astronomia "Augusto Righi" - Alma Mater Studiorum Università di Bologna, via Piero Gobetti 93/2, 40129 Bologna, Italy
[86] Department of Physics, Institute for Computational Cosmology, Durham University, South Road, Durham, DH1 3LE, UK
[87] Université Côte d'Azur, Observatoire de la Côte d'Azur, CNRS, Laboratoire Lagrange, Bd de l'Observatoire, CS 34229, 06304 Nice cedex 4, France
[88] Université Paris Cité, CNRS, Astroparticule et Cosmologie, 75013 Paris, France
[89] CNRS-UCB International Research Laboratory, Centre Pierre Binetruy, IRL2007, CPB-IN2P3, Berkeley, USA
[90] University of Applied Sciences and Arts of Northwestern Switzerland, School of Engineering, 5210 Windisch, Switzerland
[91] Institut d'Astrophysique de Paris, 98bis Boulevard Arago, 75014, Paris, France
[92] Institute of Physics, Laboratory of Astrophysics, Ecole Polytechnique Fédérale de Lausanne (EPFL), Observatoire de Sauverny, 1290 Versoix, Switzerland
[93] Aurora Technology for European Space Agency (ESA), Camino bajo del Castillo, s/n, Urbanizacion Villafranca del Castillo, Villanueva de la Cañada, 28692 Madrid, Spain
[94] Institut de Física d'Altes Energies (IFAE), The Barcelona Institute of Science and Technology, Campus UAB, 08193 Bellaterra (Barcelona), Spain
[95] School of Mathematics, Statistics and Physics, Newcastle University, Herschel Building, Newcastle-upon-Tyne, NE1 7RU, UK
[96] DARK, Niels Bohr Institute, University of Copenhagen, Jagtvej 155, 2200 Copenhagen, Denmark
[97] Waterloo Centre for Astrophysics, University of Waterloo, Waterloo, Ontario N2L 3G1, Canada
[98] Department of Physics and Astronomy, University of Waterloo, Waterloo, Ontario N2L 3G1, Canada
[99] Perimeter Institute for Theoretical Physics, Waterloo, Ontario N2L 2Y5, Canada
[100] Centre National d'Etudes Spatiales – Centre spatial de Toulouse, 18 avenue Edouard Belin, 31401 Toulouse Cedex 9, France
[101] Institute of Space Science, Str. Atomistilor, nr. 409 Măgurele, Ilfov, 077125, Romania
[102] Consejo Superior de Investigaciones Cientificas, Calle Serrano 117, 28006 Madrid, Spain
[103] Universidad de La Laguna, Departamento de Astrofísica, 38206 La Laguna, Tenerife, Spain
[104] Caltech/IPAC, 1200 E. California Blvd., Pasadena, CA 91125, USA
[105] Institut für Theoretische Physik, University of Heidelberg, Philosophenweg 16, 69120 Heidelberg, Germany
[106] Institut de Recherche en Astrophysique et Planétologie (IRAP), Université de Toulouse, CNRS, UPS, CNES, 14 Av. Edouard Belin, 31400 Toulouse, France
[107] Université St Joseph; Faculty of Sciences, Beirut, Lebanon
[108] Departamento de Física, FCFM, Universidad de Chile, Blanco Encalada 2008, Santiago, Chile
[109] Institut d'Estudis Espacials de Catalunya (IEEC), Edifici RDIT, Campus UPC, 08860 Castelldefels, Barcelona, Spain
[110] Satlantis, University Science Park, Sede Bld 48940, Leioa-Bilbao, Spain
[111] Institute of Space Sciences (ICE, CSIC), Campus UAB, Carrer de Can Magrans, s/n, 08193 Barcelona, Spain
[112] Infrared Processing and Analysis Center, California Institute of Technology, Pasadena, CA 91125, USA
[113] Instituto de Astrofísica e Ciências do Espaço, Faculdade de Ciências, Universidade de Lisboa, Tapada da Ajuda, 1349-018 Lisboa, Portugal
[114] Niels Bohr Institute, University of Copenhagen, Jagtvej 128, 2200 Copenhagen, Denmark
[115] Universidad Politécnica de Cartagena, Departamento de Electrónica y Tecnología de Computadoras, Plaza del Hospital 1, 30202 Cartagena, Spain
[116] Dipartimento di Fisica e Scienze della Terra, Università degli Studi di Ferrara, Via Giuseppe Saragat 1, 44122 Ferrara, Italy
[117] Istituto Nazionale di Fisica Nucleare, Sezione di Ferrara, Via Giuseppe Saragat 1, 44122 Ferrara, Italy
[118] INAF, Istituto di Radioastronomia, Via Piero Gobetti 101, 40129 Bologna, Italy
[119] Department of Physics, Oxford University, Keble Road, Oxford OX1 3RH, UK
[120] Instituto de Astrofísica de Canarias (IAC); Departamento de Astrofísica, Universidad de La Laguna (ULL), 38200, La Laguna, Tenerife, Spain

[121] Université PSL, Observatoire de Paris, Sorbonne Université, CNRS, LERMA, 75014, Paris, France
[122] Université Paris-Cité, 5 Rue Thomas Mann, 75013, Paris, France
[123] INAF-Osservatorio Astronomico di Brera, Via Brera 28, 20122 Milano, Italy, and INFN-Sezione di Genova, Via Dodecaneso 33, 16146, Genova, Italy
[124] ICL, Junia, Université Catholique de Lille, LITL, 59000 Lille, France
[125] ICSC - Centro Nazionale di Ricerca in High Performance Computing, Big Data e Quantum Computing, Via Magnanelli 2, Bologna, Italy
[126] Instituto de Física Teórica UAM-CSIC, Campus de Cantoblanco, 28049 Madrid, Spain
[127] CERCA/ISO, Department of Physics, Case Western Reserve University, 10900 Euclid Avenue, Cleveland, OH 44106, USA
[128] Technical University of Munich, TUM School of Natural Sciences, Physics Department, James-Franck-Str. 1, 85748 Garching, Germany
[129] Max-Planck-Institut für Astrophysik, Karl-Schwarzschild-Str. 1, 85748 Garching, Germany
[130] Laboratoire Univers et Théorie, Observatoire de Paris, Université PSL, Université Paris Cité, CNRS, 92190 Meudon, France
[131] Departamento de Física Fundamental. Universidad de Salamanca. Plaza de la Merced s/n. 37008 Salamanca, Spain
[132] Université de Strasbourg, CNRS, Observatoire astronomique de Strasbourg, UMR 7550, 67000 Strasbourg, France
[133] Center for Data-Driven Discovery, Kavli IPMU (WPI), UTIAS, The University of Tokyo, Kashiwa, Chiba 277-8583, Japan
[134] California Institute of Technology, 1200 E California Blvd, Pasadena, CA 91125, USA
[135] Department of Physics & Astronomy, University of California Irvine, Irvine CA 92697, USA
[136] Department of Mathematics and Physics E. De Giorgi, University of Salento, Via per Arnesano, CP-I93, 73100, Lecce, Italy
[137] INFN, Sezione di Lecce, Via per Arnesano, CP-193, 73100, Lecce, Italy
[138] INAF-Sezione di Lecce, c/o Dipartimento Matematica e Fisica, Via per Arnesano, 73100, Lecce, Italy
[139] Departamento Física Aplicada, Universidad Politécnica de Cartagena, Campus Muralla del Mar, 30202 Cartagena, Murcia, Spain
[140] Instituto de Física de Cantabria, Edificio Juan Jordá, Avenida de los Castros, 39005 Santander, Spain
[141] CEA Saclay, DFR/IRFU, Service d'Astrophysique, Bat. 709, 91191 Gif-sur-Yvette, France
[142] Department of Computer Science, Aalto University, PO Box 15400, Espoo, FI-00 076, Finland
[143] Dipartimento di Fisica - Sezione di Astronomia, Università di Trieste, Via Tiepolo 11, 34131 Trieste, Italy
[144] Instituto de Astrofísica de Canarias, c/ Via Lactea s/n, La Laguna 38200, Spain. Departamento de Astrofísica de la Universidad de La Laguna, Avda. Francisco Sanchez, La Laguna, 38200, Spain
[145] Ruhr University Bochum, Faculty of Physics and Astronomy, Astronomical Institute (AIRUB), German Centre for Cosmological Lensing (GCCL), 44780 Bochum, Germany
[146] Department of Physics and Astronomy, Vesilinnantie 5, 20014 University of Turku, Finland
[147] Serco for European Space Agency (ESA), Camino bajo del Castillo, s/n, Urbanizacion Villafranca del Castillo, Villanueva de la Cañada, 28692 Madrid, Spain
[148] ARC Centre of Excellence for Dark Matter Particle Physics, Melbourne, Australia
[149] Centre for Astrophysics & Supercomputing, Swinburne University of Technology, Hawthorn, Victoria 3122, Australia
[150] Department of Physics and Astronomy, University of the Western Cape, Bellville, Cape Town, 7535, South Africa
[151] DAMTP, Centre for Mathematical Sciences, Wilberforce Road, Cambridge CB3 0WA, UK
[152] Kavli Institute for Cosmology Cambridge, Madingley Road, Cambridge, CB3 0HA, UK
[153] Department of Astrophysics, University of Zurich, Winterthurerstrasse 190, 8057 Zurich, Switzerland
[154] Department of Physics, Centre for Extragalactic Astronomy, Durham University, South Road, Durham, DH1 3LE, UK
[155] IRFU, CEA, Université Paris-Saclay 91191 Gif-sur-Yvette Cedex, France
[156] Oskar Klein Centre for Cosmoparticle Physics, Department of Physics, Stockholm University, Stockholm, SE-106 91, Sweden
[157] Astrophysics Group, Blackett Laboratory, Imperial College London, London SW7 2AZ, UK
[158] Univ. Grenoble Alpes, CNRS, Grenoble INP, LPSC-IN2P3, 53, Avenue des Martyrs, 38000, Grenoble, France
[159] INAF-Osservatorio Astrofisico di Arcetri, Largo E. Fermi 5, 50125, Firenze, Italy
[160] Dipartimento di Fisica, Sapienza Università di Roma, Piazzale Aldo Moro 2, 00185 Roma, Italy
[161] Centro de Astrofísica da Universidade do Porto, Rua das Estrelas, 4150-762 Porto, Portugal
[162] HE Space for European Space Agency (ESA), Camino bajo del Castillo, s/n, Urbanizacion Villafranca del Castillo, Villanueva de la Cañada, 28692 Madrid, Spain
[163] Department of Astrophysical Sciences, Peyton Hall, Princeton University, Princeton, NJ 08544, USA
[164] Theoretical astrophysics, Department of Physics and Astronomy, Uppsala University, Box 515, 751 20 Uppsala, Sweden
[165] Minnesota Institute for Astrophysics, University of Minnesota, 116 Church St SE, Minneapolis, MN 55455, USA
[166] Mathematical Institute, University of Leiden, Einsteinweg 55, 2333 CA Leiden, The Netherlands
[167] School of Physics & Astronomy, University of Southampton, Highfield Campus, Southampton SO17 1BJ, UK
[168] Institute of Astronomy, University of Cambridge, Madingley Road, Cambridge CB3 0HA, UK
[169] Space physics and astronomy research unit, University of Oulu, Pentti Kaiteran katu 1, FI-90014 Oulu, Finland
[170] Center for Computational Astrophysics, Flatiron Institute, 162 5th Avenue, 10010, New York, NY, USA
[171] Department of Physics and Astronomy, University of British Columbia, Vancouver, BC V6T 1Z1, Canada